CrystEngComm

Correlation of Solid-State Order to Optoelectronic Behavior in Heterocyclic Oligomers

Journal:	*CrystEngComm*
Manuscript ID	CE-ART-04-2022-000560.R1
Article Type:	Paper
Date Submitted by the Author:	26-May-2022
Complete List of Authors:	Karunathilaka, Dilan ; University of Mississippi, Chemistry & Biochemistry Rajapakse, R.; University of Peradeniya, Chemistry Steen, April; University of Mississippi, Chemistry and Biochemistry Sexton, Thomas ; University of Mississippi, Chemistry and Biochemistry; Valley City State University Sparks, Nicholas; University of Mississippi, Chemistry & Biochemistry Mosely, Jacquelyn ; University of Mississippi, Chemistry and Biochemistry Rheingold, Arnold; University of California, Department of Chemistry and Biochemistry Hammer, Nathan; University of Mississippi, Chemistry & Biochemistry Tschumper, Gregory; University of Mississippi, Department of Chemistry and Biochemistry Watkins, Davita; University of Mississippi, Chemistry and Biochemistry

ARTICLE

Correlation of Solid-State Order to Optoelectronic Behavior in Heterocyclic Oligomers

Received 00th January 20xx,
Accepted 00th January 20xx

DOI: 10.1039/x0xx00000x

Dilan Karunathilaka [a], R.M.G. Rajapakse [a], April E. Hardin [a], Thomas More Sexton [a†], Nicholas E Sparks [a], Jacquelyn J. Mosely [a], Arnold L. Rheingold [b], Nathan I. Hammer [a], Gregory S. Tschumper [a], and Davita L. Watkins [a*]*

A longstanding challenge in the field of optoelectronic materials, the effects of solid-state arrangement and morphology are still a prominent factor associated with small-molecule and polymer-based device performance. Here, mixed heterocyclic aromatic oligomers containing thiophene, furan and pyrazine are prepared alongside their methylated congeners. Their solution and solid-phase properties were studied via spectroscopic, electrochemical and single-crystal (X-ray diffraction) XRD analysis. Comparative analysis between solid-state packing arrangements and photophysical properties revealed optical band gaps as low as 1.7 eV with Stokes-shifts up to 130 nm and quantum yields of 12%. Results of the study aid in further understanding the effects of molecular and solid-state arrangements that give rise to unique optical and photophysical properties critical to enhancing optoelectronic behavior.

Introduction

Organic optoelectronic materials, including electronically conducting polymers and oligomers, are a class of materials that have profoundly impacted the field of semiconducting devices.[1-3] One of the main advantages of organic polymers and oligomers over their inorganic counterparts is their versatility for designing innumerable different materials. This can be done by covalently linking heterocyclic aromatic compounds in an order to result in tailor-made materials with distinctive properties.[4, 5] The use of small molecules and/or oligomers is ideal as they are often comprised of convenient and tuneable building blocks whose solvent-dependent self-assembly in the solution phase and highly ordered assembly in the solid-state can be readily studied by optical, electrochemical, and computational means. The latter is significant as solid-state order can lead to perfectly defined crystals and bulk materials depending on intra-molecular, inter-molecular, and/or solvent-solute interactions affording architectures with highly impressive optical and electronic properties.[6-8]

Due to their important role in charge transfer and conductivity, organic π-conjugated oligomers have been the topic of significant research. Optoelectronic molecules' function depends on their extended π conjugation and tunability of the chemical composition. The electronic coupling between neighboring molecules, which is contingent upon the solid-state organization, significantly impacts charge transfer mobilities. Therefore, solid-state structure plays an important role in optoelectronic device performance and understanding the solid-state order of the organic building blocks that make up the device is crucial to the advancement.

Chalcogen-based heterocycles are amongst the most extensively studied building blocks for organic optoelectronic devices.[9] Thiophene-based materials have been studied to a great extent for optical and electronic applications due to their high stability, good electron transport capability, and synthetic accessibility.[10, 11] Due to the non-covalent intermolecular interactions of these thiophene-based materials, they tend to self-order in solution state and solid-state, leading to their optical and electronic properties.[12] In comparison, furan has been shown to have better solubility, tighter solid-state packing, high photoluminescence quantum yields, and immense charge delocalization.[13-15] Like others in the field, we have found that co-oligomers and mixed hetero-oligomers of furan and thiophene exhibit different optical properties despite the structural resemblance.[16-19] In this sense, these co-oligomer systems with both heterocycles adopt the advantages of each ring while counterbalancing their adverse effects.

Here we conducted a comparative analysis correlating the solid-state structure of four oligomers containing pyrazine-bithiophene to that of the chemical and photophysical properties. The oligomers of interest 2,5-bis(5'-hexyl-[2,2'-bithiophen]-5-yl)pyrazine (**Pyrz(TT)$_2$**), 2,5-bis(5'-hexyl-[2,2'-bithiophen]-5-yl)-3,6-dimethylpyrazine (**MePyrz(TT)$_2$**), and mixed thiophene and furan 2,5-bis(5-(5-hexylthiophen-2-

[a] *Department of Chemistry and Biochemistry, University of Mississippi, University, MS 38677-1848, USA; corresponding author emails: tschumpr@olemiss.edu; dwatkins@olemiss.edu*
[b] *Department of Chemistry, University of California, San Diego, La Jolla, CA 92093-0358, USA*

† Current address: Department of Science, Valley City State University, Valley City, ND 58072.
Electronic Supplementary Information (ESI) available: [details of any supplementary information available should be included here]. See DOI: 10.1039/x0xx00000x

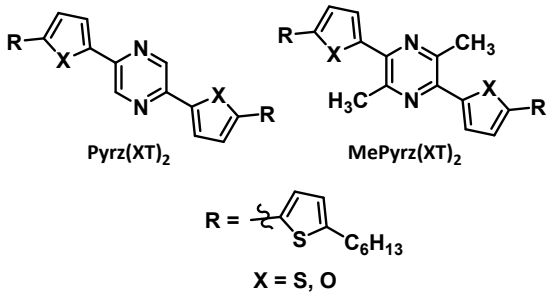

Figure 1. Molecular structures of four synthesized compounds **Pyrz(FT)$_2$**, **Pyrz(TT)$_2$**, **MePyrz(FT)$_2$**, and **MePyrz(TT)$_2$**).

yl)furan-2-yl)pyrazine (**Pyrz(FT)$_2$**), 2,5-bis(5-(5-hexylthiophen-2-yl)furan-2-yl)-3,6-dimethylpyrazine (**MePyrz(FT)$_2$**) co-oligomers are shown in Figure 1.

The oligomers consist of a pyrazine core flanked with either bithiophene or 2-(thiophen-2-yl)furan side groups (**Pyrz(FT)$_2$** and **Pyrz(TT)$_2$**). Pyrazines have emerged as leading components in push-pull and donor-acceptor functionalized materials. Its electron-deficient character and molecular tunability make it a suitable π-linker, with its nitrogen providing an attractive center for supramolecular complexations. The hexyl chains were introduced to increase the solubility of the compound in organic solvents. In comparison, two methylated compounds **MePyrz(FT)$_2$** and **MePyrz(TT)$_2$** were synthesized and studied to improve solid-state packing and enhance optical properties compared to the two unsubstituted forms (Fig. 1).[20, 21] The synthesis, electrochemical and optical properties in the solution and solid phase are described. By comparing the structure and solid-state arrangements that contribute to photophysical properties of these oligomers, tailor-made optical materials containing furan, thiophene, and pyrazine are presented for applications in optoelectronic devices.

EXPERIMENTAL SECTION

Reagents and solvents such as toluene (PhMe) and acetonitrile (ACN) were purchased from commercial sources and used without further purification unless otherwise specified. Additional synthetic details, structural figures, TG/DTA plots, and X-ray crystallographic tables containing bond distances and angles can be found in the Supporting Information (SI).

Synthesis

Tetrahydrofuran (THF), ether, dichloromethane (DCM), and dimethylformamide (DMF) were degassed in 20 L drums and passed through two sequential purification columns (activated alumina; molecular sieves for DMF) under a positive argon atmosphere. Thin-layer chromatography (TLC) was performed on SiO_2-60 F254 aluminum plates with visualization by ultraviolet (UV) light or staining. Flash column chromatography was performed using Purasil SiO_2-60, 230–400 mesh from Whatman. Additional synthetic details can be found in the SI.

Theoretical Methods

In order to gain insight into the structural, optoelectronic, and vibrational properties of each oligomer, depicted in Figure 1, full geometry optimizations and corresponding harmonic vibrational frequency computations were performed with the global hybrid B3LYP [22-24] density functional in conjunction with a split-valence triple-ζ quality 6-311G(2*df*, 2*pd*) basis set.[25, 26] A subsequent set time-dependent density functional theory (TD-DFT) [27-30] single-point energy computations, at the same level of theory, were performed in order to quantify the theoretical absorption and emission spectra, Frank-Condon HOMO-LUMO energy gaps (E_{HL}) and vertical S_0 to S_1 excitation energies ($E^{vert}_{1\leftarrow 0}$). This TD-DFT approach was also used to re-optimize each ground state minimum on the S1 excited state surface to gain greater insight into the structural and optoelectronic properties of the lowest energy excited state structure of each oligomer.

Electrochemical Analysis

Cyclic voltammetry (CV) measurements were performed on a CH Instruments CHI-610E Electrochemical Analyzer potentiostat/galvanostat. All CVs were collected under an argon blanket with doubly distilled DCM which was degassed with argon just before use. 0.10 mol dm^{-3} tetrabutylammonium hexafluorophosphate (Bu_4NPF_6) was used as the background electrolyte. A glassy carbon working electrode, platinum-wire counter electrode, and a saturated calomel reference electrode (SCE) were used. Unless otherwise stated, all potentials are quoted with respect to (wrt) SCE. In order to obtain the LUMO and HOMO levels of compounds from CV data, CVs were run, starting from 0 V where there was no appreciable current, towards the negative direction (up to about – 1.5 V) and in the positive direction (up to about + 1.5 V) separately and the corresponding potentials E_{red} and E_{ox} were identified as the potentials of LUMO and HOMO, respectively. Potentials were converted to the energies in eV and are quoted wrt vacuum level and the correction factors recommended for converting electronic energies in aqueous solutions to those in non-aqueous solutions were used as per IUPAC recommendation.[31]

Spectroscopic Analysis

Solutions of each of the four compounds were created using either HiPerSolv CHROMANORM toluene from BDH Analytical Chemicals or spectroscopic grade DCM and DMF from Fisher Scientific. To promote the dissolution of solid, gentle sonication was performed for 15 minutes. Argon was bubbled through each solution for one minute to remove oxygen. Solutions were prepared immediately before performing spectroscopic analyses.

UV-Vis absorption spectra were obtained using an Agilent 5000 UV-Vis NIR spectrometer. Solid-state absorbance (diffuse reflectance) spectra were obtained by directing light from a Xenon arc lamp onto the sample, which was placed inside a Stellar Net Inc. IC2 integrating sphere. The reflected light was collected using a solarization-resistant fiber optic cable and was directed into an Ocean Optics USB2000 spectrometer for analysis. The obtained spectra were compared to a standard of

Spectralon® to calculate the percent reflectivity, and these values were used in conjunction with the Kubelka-Munk function to generate the diffuse reflectance spectra.[32,33]

The fluorescence emissions for the solid- and solution-states were obtained using a Nikon TE2000U inverted microscope and CCD detection with a 405 nm ps pulsed diode laser. All solutions were created at 10^{-5} M concentration in DCM. Excited-state lifetimes were also obtained using a Nikon TE2000U inverted microscope and a PMD series single photon avalanche diode from PicoQuant with a 50 ps timing resolution in conjunction with a pulsed 405 nm ps diode laser. These values were fit to exponential decay functions in order to calculate the lifetimes. Merged diagrams of optical profiles are located in the SI for comparison.

X-ray Crystallography

Crystals were prepared by dissolving each oligomer separately in a chlorinated solvent (DCM or chloroform) and adding it dropwise to a borosilicate glass vial. The open vial was placed in a secondary vial containing *n*-hexane. Using vapor diffusion methods, the solvent was allowed to evaporate at -5 °C over 8 days until the formation of crystals. Crystal evaluation and data collection were performed on a Bruker Kappa diffractometer with Mo Kα (λ = 0.71073 Å) radiation. Reflections were indexed by an automated indexing routine built in the APEXII program suite. The solution and refinement were carried out in Olex2 version 1.2 using the program SHELXTL. [34, 35] Non-hydrogen atoms were refined with anisotropic thermal parameters, while hydrogen atoms were introduced at calculated positions based on their carrier/parent atoms. The single crystal X-ray structure of the co-crystal CCDC numbers are 2168005, 2168006, 2168007 and 2168008. Crystal data and structure refinement parameters for all compounds are given in the SI.

Computational Analysis

Figure 2 shows the computed photophysical properties of the oligomers in a graphical form. Terminal hexyl groups were replaced by methyl groups in the computational analysis.

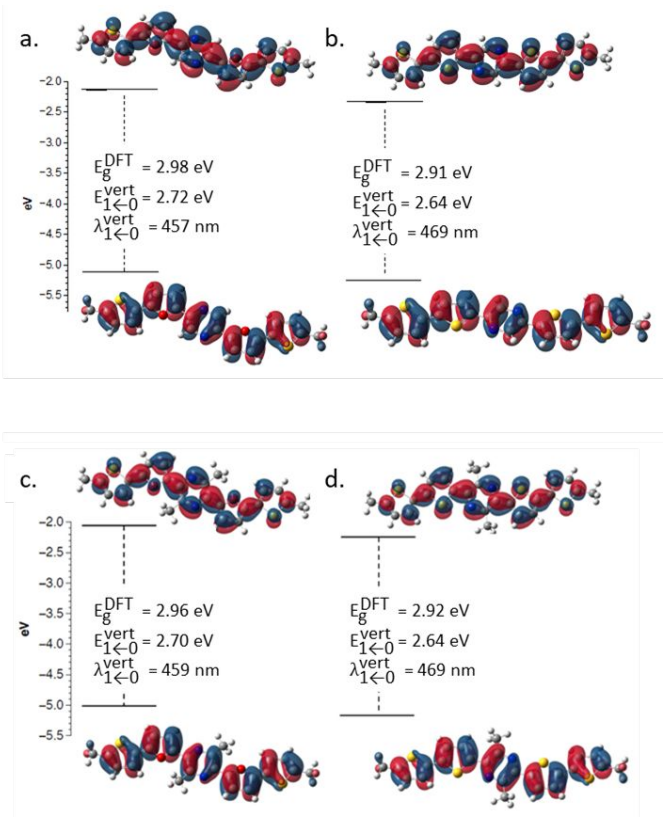

Figure 2. Optimized geometries and highest singly or doubly occupied molecular orbitals (HOMOs) of (a) ground S_0 state (C_{2h}) and first excited S_1 state (C_{2h}) of **Pyrz(FT)$_2$**, (b) ground S_0 state (C_i) and first excited S_1 state (C_{2h}) of **Pyrz(TT)$_2$**, (c) ground S_0 state (C_{2h}) and first excited S_1 state (C_{2h}) of **MePyrz(FT)$_2$**, (d) ground S_0 state (C_i) and first excited S_1 state (C_{2h}) of **MePyrz(TT)$_2$**

Results and Discussion

Oligomer Synthesis

Preparation of the target oligomers primarily followed literature reported preparation of similar derivatives.[36, 37] Scheme S1 shows the synthetic route for the four oligomers. We began our synthesis by achieving compound 4, which started from the bromination of 2-hexylthiophene (compound 1) followed by standard Stille coupling and stannylation, correspondingly. Compound 9 was synthesized by starting from commercially available alanine anhydride and reacted with phosphoryl chloride ($POCl_3$), followed by phosphoryl bromide ($POBr_3$). Mixed heterocycles or thiophene-furan derivatives were synthesized via Stille coupling of compounds 4 with compounds 5 and 9, giving **Pyrz(FT)$_2$** a 15% yield and **MePyrz(FT)$_2$** in a 35% yield. Bithiophene derivatives were synthesized by Suzuki coupling between commercially available compound 6 with compounds 5 and 9 to give **Pyrz(TT)$_2$** in 65% yield and **MePyrz(TT)$_2$** in 55% yield, respectively. ^{1}H NMR and ^{13}C NMR confirmed the structural integrity of each oligomer. A full synthetic description is included in the SI.

The structures of these 8 optimized geometries are also provided in the SI without the orbital overlays along with the corresponding Cartesian coordinates.

The lowest energy conformations for the electronic ground state (S_0) and the first excited state (S_1) of **Pyrz(FT)$_2$**, **Pyrz(TT)$_2$**, **MePyrz(FT)$_2$**, and **MePyrz(TT)$_2$** are shown in Figure 2. The lowest energy conformation of S_0 **Pyrz(FT)$_2$** has heteroatoms *trans* for each inter-ring bond. Both S_0 and S_1 are planar for **Pyrz(FT)$_2$** with C_{2h} symmetry. A second energetically competitive conformation of **Pyrz(FT)$_2$** has thiophene and furan in *cisoid* configuration. This configuration is nearly equal in energy to the *transoid* configuration (+0.02 kcal mol^{-1}), as previously seen in the literature for thiophene/furan oligomers.[38, 39] The photophysical properties computed for this *cisoid* conformer are nearly identical to those reported in Figure 2a for the *transoid* global minimum.. **MePyrz(FT)$_2$** has the same lowest energy conformation as **Pyrz(FT)$_2$** for both S_0 and S_1. Like **Pyrz(FT)$_2$**, **MePyrz(FT)$_2$** has a second energetically competitive conformation with thiophene and furan in *cisoid* configuration

(+0.11 kcal mol^{-1}) again with nearly the same photophysical properties as the corresponding global minimum (Figure 2c).

For **Pyrz(TT)$_2$** and **MePyrz(TT)$_2$**, the heteroatoms of the 5-membered rings also adopt *trans* orientations with respect to each other in their lowest energy conformations on S0. In contrast, the cis orientation of the S atoms of the inner thiophene rings relative to the N atoms of the central pyrazine ring differs from that of the furan rings in **Pyrz(FT)$_2$** and **MePyrz(FT)$_2$**.

Table 1. Electrochemical data, theoretical absorption and emission data

	Electrochemical			Theoretical				
				Absorption			Emission	
	HOMO (eV)	LUMO (eV)	E_g^{CV} (eV)	λ^{abs} (nm)	E_g^{DFT} (eV)	$E_{1\leftarrow0}^{vert}$ (eV)	λ^{ems} (nm)	Stokes Shift (eV)
Pyrz(FT)$_2$	-5.87	-3.78	2.09	457	2.98	2.72	509	0.27
Pyrz(TT)$_2$	-5.76	-3.54	2.22	469	2.91	2.64	533	0.31
MePyrz(FT)$_2$	-5.8	-3.69	2.11	459	2.96	2.70	514	0.29
MePyrz(TT)$_2$	-5.89	-3.65	2.24	469	2.92	2.64	534	0.32

Estimated from the empirical equation $HOMO^{CV}$ = -(5.10 + Eonset) (eV)

The SCCS dihedral between adjacent thiophene moieties in **Pyrz(TT)$_2$** is 164.9 degrees, while the central three heterocycles are nearly planar (SCCN dihedral of only 0.4 degrees), and the complex has C_i symmetry. In addition, the fully planar form is only 0.05 kcal mol^{-1} higher in energy than the non-planar form, with similar computed absorption properties. In contrast to S_0, the first excited state S_1 for **Pyrz(TT)$_2$** is planar with C_{2h} symmetry. For both oligomers, inter-ring bond lengths between thiophenes in the excited state are shorter by 0.02-0.03 Å than those in the ground state. This contraction is consistent with increased π-bonding character for these bonds in the excited state, as observed from the orbital analysis (*vide infra*) for both molecules and the planarity of S_1 for **Pyrz(TT)$_2$**. Nearly identical results are seen for **MePyrz(TT)$_2$** as for **Pyrz(TT)$_2$**.

The highest doubly or singly occupied molecular orbital for S_0 and S_1, respectively, is shown in Figure 2 for each oligomer (simply denoted HOMO). For each optimized S_0 geometry, the fundamental gap was approximated by Koopman's theorem (giving E_g^{DFT}) and by TD-DFT (giving $E_{1\leftarrow0}^{vert}$), (Table 1). The λ^{abs} is found by converting $E_{1\leftarrow0}^{vert}$ to nm while λ^{ems} is found by TD-DFT computations on the S_1 optimized geometry. The HOMOs for both S_0 and S_1 show primarily π-character spanning the entire molecule for each oligomer, with the S_0 HOMO showing nodal surfaces between the rings. In contrast, the S_1 HOMO shows π-bonding character between each pair of adjacent thiophene rings supporting the co-planarity of the rings in the S1 optimized geometries of **Pyrz(TT)$_2$** and **MePyrz(TT)$_2$**. These results are consistent with our previous photophysical study on furan and thiophene-containing oligomers.[40]

Electrochemical Analysis

Cyclic voltammetry was used to study the redox properties of the oligomers and to obtain the electrochemical HOMO-LUMO gaps for each oligomer. Band gap values for all oligomers are smaller than that those predicted via theoretical data. These values result from poor solubility and aggregation/deposition of solid molecules onto the working electrode. These values due correlate well with solid-state results (*vide infra*) and support this claim.

Considering the cyclic voltammogram of **Pyrz(FT)$_2$** (S12a), the first oxidation in the positive direction can be assigned to the oxidation of the pyrazine ring, forming TF-Pyrz$^+$-FT. This potential is assigned to the HOMO of the molecule, which corresponds to +1.072 V with respect to (wrt) saturated calomel electrode (SCE) and it is calculated as -5.87 eV (Table 1) wrt vacuum level.[41] The LUMO of **Pyrz(FT)$_2$** can be studied via regeneration of the pyrazine ring by the addition of an electron to its excited state at -1.013 V wrt SCE and -3.78 eV wrt vacuum level. This gives rise to a 2.09 eV HOMO-LUMO gap for **Pyrz(FT)$_2$**. HOMO value of the **Pyrz(TT)$_2$** is found to be +0.961 V wrt SCE and -5.76 eV wrt vacuum level, while LUMO at -1.043 V wrt SCE and -3.54 eV wrt vacuum level, which leads to a 2.22 eV HOMO-LUMO gap. Similarly, the HOMO-LUMO gap for methylated compounds is also calculated. **MePyrz(FT)$_2$** shows its HOMO at +1.002 V wrt SCE and -5.80 eV wrt vacuum level. The LUMO of **MePyrz(FT)$_2$** was found to be at -1.112 V wrt SCE and -3.69 eV wrt vacuum level. This will lead to a 2.11 eV HOMO-LUMO gap for **MePyrz(FT)$_2$**. Accordingly, HOMO-LUMO gap for **MePyrz(TT)$_2$** was calculated to be 2.24 eV.

The redox chemistry of the furan-containing compounds appeared at a relatively shorter potential window than that of the two thiophene-containing compounds. Since furan has the more electronegative oxygen atom compared to that of the sulfur atom present in thiophene, the furan-containing derivatives tend to withdraw more electrons from the pyrazine core, making the pyrazine core in the furan-containing compounds more receptive to oxidation. Therefore, furan-containing compounds show a lower HOMO-LUMO gap for both the standard and methylated versions. The electron-donating capabilities of the two methyl groups increase the electron density on the pyrazine ring, leading to the pyrazine being less receptive to oxidation. It should show a higher potential window for methylated compounds and this can be seen in **MePyrz(FT)$_2$** and **MePyrz(TT)$_2$**, which have higher HOMO-LUMO gaps (2.11 eV and 2.24 eV) compared to their standard versions, which have HOMO-LUMO gaps of 2.09 eV and 2.24 eV, respectively.

Spectroscopic Analysis

The photophysical properties of compounds were studied by absorption and emission spectroscopy in DCM (Fig. 3 and Fig. 4). As outlined in Figures 3 and Table 2, higher λ_{max}^{abs} and λ_{max}^{em} values can be observed for TT analog compared to FT analog with an exception in the λ_{max}^{em} for **Pyrz(FT)$_2$**. The trend observed here in regards to λ_{max}^{abs} is **MePyrz(FT)$_2$** (393 nm) **< Pyrz(FT)$_2$** (431 nm) **< MePyrz(TT)$_2$** (435 nm) **< Pyrz(TT)$_2$** (439 nm). While trend for λ_{max}^{em} is **MePyrz(FT)$_2$** (494 nm) **< MePyrz(TT)$_2$** (495 nm) **<**

Table 2. Solution state and solid-state absorption and emission data

	Solution					Solid					
	Absorbance			Emission		Absorbance			Emission		QY (%)
	λ_{max} (nm)	λ_{onset} (nm)	E_g (eV)	λ_{max} (nm)	Stokes shift (eV)	λ_{max} (nm)	λ_{onset} (nm)	E_g (eV)	λ_{max} (nm)	Stokes shift (eV)	
$Pyrz(FT)_2$	431	486	2.55	506	0.46	516	730	1.70	613	0.38	<1
$Pyrz(TT)_2$	439	490	2.53	501	0.35	495	560	2.21	549	0.25	9
$MePyrz(FT)_2$	393	478	2.59	494	0.64	417	527	2.35	547	0.71	5
$MePyrz(TT)_2$	435	489	2.53	495	0.34	493	553	2.24	547	0.25	12

10^{-5} M concentration in DCM; bandgap [Energy (hv) = 1240/onset wavelength(nm)]; merged diagrams of optical profiles are located in the SI for comparison (Fig. S21).

$Pyrz(TT)_2$ (501 nm) **< $Pyrz(FT)_2$** (506 nm)**.** This trend can be correlated with the theoretical data where **$Pyrz(TT)_2$** and **$MePyrz(TT)_2$** have higher λ_{max}^{abs} and λ_{max}^{em} values compared to its TF analog.

Using the absorption onset values, optical bandgaps were calculated. Calculated optical band gap values are higher for **$Pyrz(FT)_2$** (2.55 eV) and **$MePyrz(FT)_2$** (2.59 eV) compared to TT analogs (2.53 eV in both TT). These values correspond to the energy of the lowest electronic transition accessible via absorption of a single photon.[42]

Interestingly, we see an increase in Stokes-shift for both **$MePyrz(FT)_2$** (+13 nm, +0.11 eV) and **$Pyrz(FT)_2$** (+41 nm, 0.30 eV) compared to TT compounds, which was not predicted via

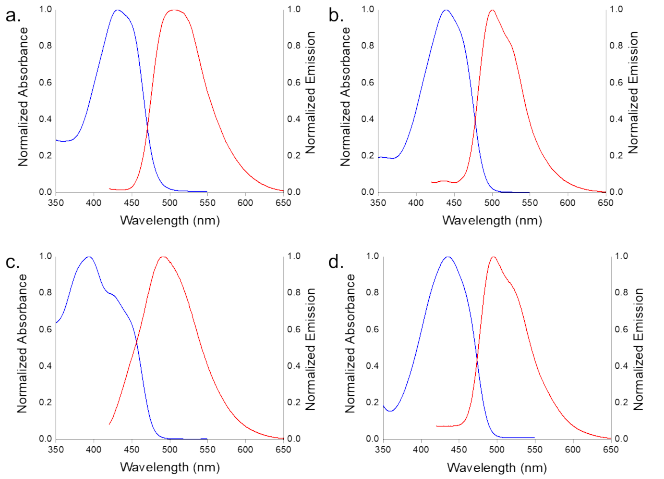

Figure 3. Solution-state absorption/fluorescence spectra of (a) **$Pyrz(FT)_2$** (b) **$Pyrz(TT)_2$** (c) **$MePyrz(FT)_2$** (d) **$MePyrz(TT)_2$** in DCM where absorbance (blue trace) and emission (red trace).

theory. An enhanced Stokes-shift can be due to several photophysical causes such as low reorganization energy, intramolecular charge transfer (ICT), and excimer formation.[43] This increase in Stokes-shift is presumably due to the latter as well as increased rigidity of **$MePyrz(FT)_2$** and **$Pyrz(FT)_2$** relative to **$Pyrz(TT)_2$** and **$MePyrz(TT)_2$**.[44] The incorporation of furan has been shown to induce a more planar and rigid molecular framework when compared to the solely thiophene-containing molecule.[45] Additionally, the comparatively smaller oxygen present in furan relative to the sulfur present in thiophene leads to an increase in intramolecular hydrogen bonding that can occur between the pyrazine hydrogen and the oxygen in furan. These intramolecular interactions can also contribute to a more planar rigid structure in the **$Pyrz(FT)_2$** and **$MePyrz(FT)$** and eventually will lead to higher Stokes-shift (75 nm, 0.46 eV and 101 nm, 0.64 eV) compared to **$Pyrz(TT)_2$** (62 nm, 0.35 eV) and **$MePyrz(TT)_2$**.[46]

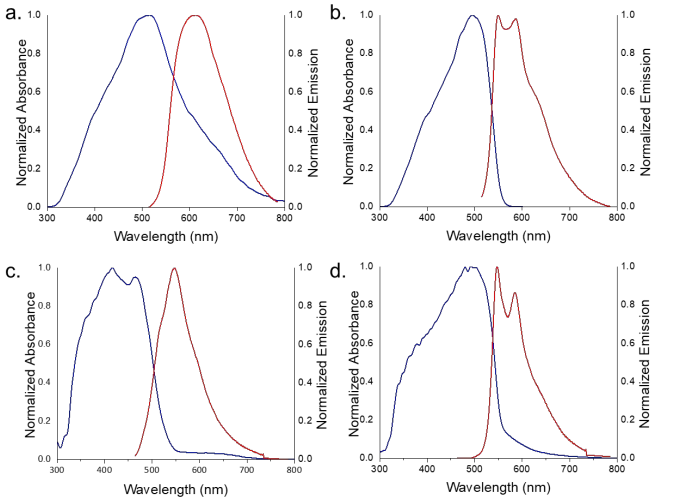

Figure 4. Solid-state diffuse reflectance and fluorescence spectra of (a) **$Pyrz(FT)_2$** (b) **$Pyrz(TT)_2$** (c) **$MePyrz(FT)_2$** (d) and **$MePyrz(TT)_2$** where diffuse reflectance (blue trace) and emission (red trace).

Relative to the TT analogs, peak broadening and blue-shifting in the solution-state λ_{max}^{abs} for **$MePyrz(FT)_2$** (393 nm) and **$MePyrz(TT)_2$** (435 nm) were observed (Fig. 3 c,d). We suspect that in the solution state, methylated derivatives are not planar. With free rotation occurring in solution, the presence of a methyl group in pyrazine induces angle and steric strain between the pyrazine and adjacent five-member

Table 3. X-ray crystallographic data for heterocyclic oligomers; additional crystal data in SI

Co-crystal	Pyrz(TT)$_2$	MePyrz(TT)$_2$	Pyrz(FT)$_2$	MePyrz(FT)$_2$
Formula	C_{32} H_{36} N_2 S_4	C_{34} H_{40} N_2 S_4	C_{32} H_{36} N_2 O_2 S_2	C_{34} H_{40} N_2 O_2 S_2
M (g/mol)	576.87	604.92	544.75	572.80
Temperature (K)	100.0	100.0	100.0	100.1
Space group	P 2_1/c	P$\bar{1}$	P 2_1/c	P$\bar{1}$
a (Å)	26.416(3)	5.765(3)	16.494(15)	5.1067(9)
b (Å)	5.6442(5)	7.688(4)	4.7436(4)	7.1680(8)
c (Å)	29.724(3)	18.142(9)	18.981(18)	20.766(3)
α (deg)	90.00	80.69	90.00	80.48
β (deg)	103.3	84.69	106.9	86.86
γ (deg)	90.00	71.68	90.00	86.42
V (Å^3)	4312.5	752.4	1420.7	747.4
Z	6	1	2	1
R factor (%)	5.30	11.30	5.16	3.94

heterocycle. This distortion in the conjugated backbone will affect electron delocalization and give access to additional conformational isomers, yielding broadening and a blue shift in its absorbance maxima.[47]

Solid-state absorbance and emission spectra (Fig. 4) were obtained and compared to solution data. As expected, (Table 2), all absorbance and emission maxima values are red-shifted and broadened. This is generally due to more significant intermolecular interactions that arise from increased planarity and tighter packing between conjugation molecules present in the solid-state.[48, 49]

Lower absorption maxima and higher bandgaps are seen for **MePyrz(FT)$_2$** (417 nm, 2.35 eV) and **MePyrz(TT)$_2$** (493 nm, 2.24 eV) compared to **Pyrz(FT)$_2$** (516 nm, 1.7 eV) and **Pyrz(TT)$_2$**. (495 nm, 2.21 eV). This agrees well with the electrochemically determined HOMO-LUMO gaps, most likely due to aggregation of oligomers on the electrode surface. Interestingly, two well resolved peaks near 600 nm were noted for the emission spectra of the thiophene-based oligomers. Such features arise from vibronic resolution and/or due to multiple low-lying energy levels.

As seen earlier with the solution state data, compared to TT analog, **Pyrz(FT)$_2$** and **MePyrz(FT)$_2$** show a higher Stokes-shift (+43 nm, +0.13 eV and +76 nm, +0.46 eV respectively) in solid state as well. This can also be explained considering the planarity and rigidity of the molecules where the replacement of thiophene with furan can reduce the dihedral angle within the conjugated framework resulting in extended conjugation, increased delocalization, and tighter packing (i.e., decreasing π-π distances between molecules) compared to the thiophene derivatives. Additionally, we also see the effects of the methyl substituent. In this case, the methyl groups would presumably increase the π-π stacking distances between conjugated frameworks, contributing to a higher bandgap.

Considering the further application of the materials as semiconductors, the quantum yields and fluorescence lifetimes for the solid-state materials were assessed. **Pyrz(FT)$_2$** has the lowest quantum yield (<1%). Alternatively, its methylated derivative, which is expected to yield higher π-π stacking distances (i.e., decreased π-π distances between molecules) compared to its standard version, shows a 5% quantum yield. **Pyrz(TT)$_2$** and **MePyrz(TT)$_2$** show higher quantum yields, comparatively.

Fluorescence emission decay curves for all oligomers exhibited biexponential lifetimes in the solid-state (Fig. S##). For **Pyrz(FT)$_2$**, a biexponential lifetime of 0.47 ns and 2.59 ns with amplitudes of 0.7 and 0.3 respectively (where the short lifetime contributes 70% to the average lifetime detected and the long lifetime contributes 30%) was obtained. For **Pyrz(TT)$_2$**, a biexponential lifetime was also observed; the shorter lifetime of 0.59 ns was found to have an amplitude of 0.9 while the longer lifetime of 1.81 ns was found to have an amplitude of 0.1. **MePyrz(FT)$_2$** was found to have a short lifetime of 1.12 ns with an amplitude of 0.8 and a long lifetime of 3.56 ns with an amplitude of 0.2. **MePyrz(TT)$_2$** was found to have a short lifetime of 0.72 ns with an amplitude of 0.9 and a long lifetime of 3.20 ns with an amplitude of 0.1. Both the long and short lifetimes of the methylated compounds were found to be longer than was observed in their unmethylated analogues. These difference as well as the biexponential lifetimes in the solid-states arise due to variations in molecular rigidity and increased intermolecular interactions in the solid causing a reduction in intermolecular distance, allowing for the formation of excimers.

X-Ray Crystallography

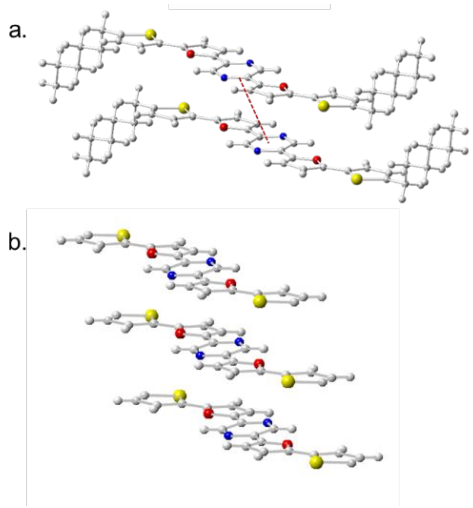

Figure 5. (a) Packing diagram conveying π-stacking of **Pyrz(FT)$_2$**; (b) co-facial alignment of π-framework of **Pyrz(FT)$_2$**; red dotted lines correspond to centroid-centroid distance

To support results from solid-state, crystal data for the oligomers were obtained, and a summary of the crystallographic data is provided in Table 3. For this study, we assess both the plane to plane and centroid to centroid distances, where the interaction between two parallel

heterocyclic frameworks molecules occurs if centroid–centroid distance <6.0 Å and the distance between the planes of interacting molecules is <4.0 Å (Table S21).[50, 51]

A clear trend in quantum yield—in which **Pyrz(FT)$_2$** and **MePyrz(FT)$_2$** exhibited lower quantum yields—can be correlated with rigidity and packing patterns between molecules in the solid-state where solid-state arrangement can lead to fluorescence quenching
due to a transfer of energy to the surrounding or adjacent molecules rather than releasing that energy as light.[52]

The unit cell structure reveals that **Pyrz(FT)$_2$** molecules pack in a co-facial manner with a crystallization that is in the monoclinic P $2_1/c$ space group (Fig. 5). The crystal structure also reveals that **Pyrz(FT)$_2$** is more planar than the other derivatives having a dihedral angle of 179.1° between the pyrazine core and furan unit. These overall characteristics of **Pyrz(FT)$_2$** lead to a packing arrangement that possesses a comparatively tighter π-π stacking distance of 3.57 Å (from plane to plane) and centroid-centroid distance of 4.74 Å relative to **Pyrz(TT)$_2$**, **MePyrz(TT)$_2$**, and **MePyrz(FT)$_2$**. This packing arrangement correlates well with its lower quantum yield (<1%).

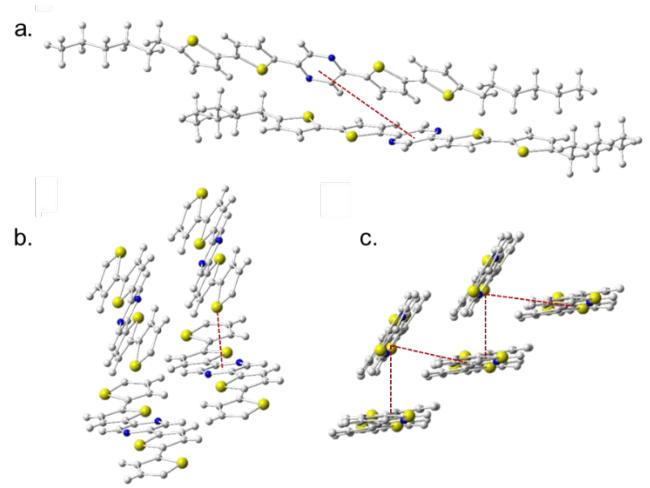

Figure 6. (a) Packing diagram conveying π-stacking of **Pyrz(TT)$_2$**; (b) Crystal fragment detailing the secondary interactions that afford a herringbone arrangement of **Pyrz(TT)$_2$;** red dotted lines correspond to centroid-centroid distance (a), sulfur-π interactions (b), and plane to plane distances (c)

Like **Pyrz(FT)$_2$**, **Pyrz(TT)$_2$** yields crystals in the monoclinic P $2_1/c$ space group where T-shaped π-stacking between molecules that leads to herringbone packing (Fig. 6).[38] Having thiophene in place of furan affords a dihedral angle of 174.5° between thiophene and pyrazine. There is a reduction in planarity and rigidity compared to **Pyrz(FT)$_2$**. The herringbone structure is considered more favorable for emission and leads to a higher quantum yield for the **Pyrz(TT)$_2$**.[53] Interestingly, the S of thiophene and N of pyrazine are in a *cisoid* arrangement with both heteroatoms on the same side. Such a four-membered arrangement would be considered unfavorable due to lone-pair repulsion and strain. However, this orientation suggests chalcogen bonding of the sulfur atom with the nitrogen in an adjacent molecule (2.94 Å) and/or long-range sulfur-π interactions (3.22 Å).

Computational investigation of 2-(2-thienyl)-pyrazine shows the *cisoid* arrangement as 1 kcal/mol lower in energy than the *transoid* arrangement, indicating that the *cisoid* arrangement is indeed energetically favorable even when not constrained by the crystal (SI). Further computational examination shows that the preference for S-C-C-N *cisoid* configuration is not affected by the S-π interaction between pyrazine and the thiophene of an adjacent molecule in the crystal orientation.

Relative to the unsubstituted derivatives, the methyl group on **MePyrz(TT)$_2$** and **MePyrz(FT)$_2$** induces larger π-π stacking distances and reduced planarity, as evident from the crystal and solid-state spectroscopic data. **MePyrz(FT)$_2$** yields crystals in the

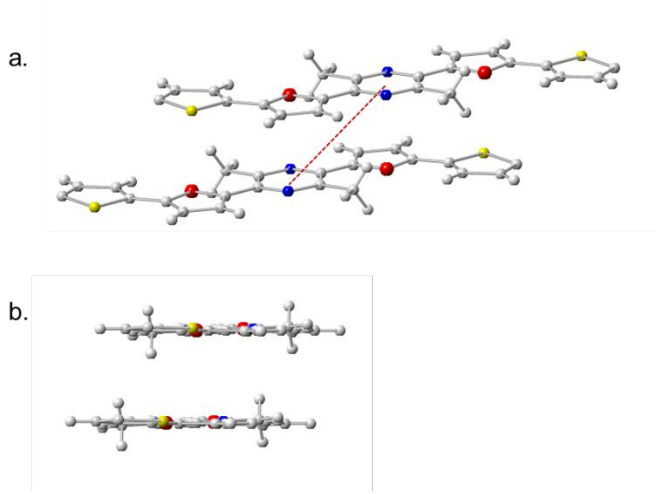

Figure 7. (a) Packing diagram conveying π-stacking of **MePyrz(FT)$_2$**; (b) co-facial alignment of π-framework of **MePyrz(FT)$_2$;** red dotted lines correspond to centroid-centroid distance

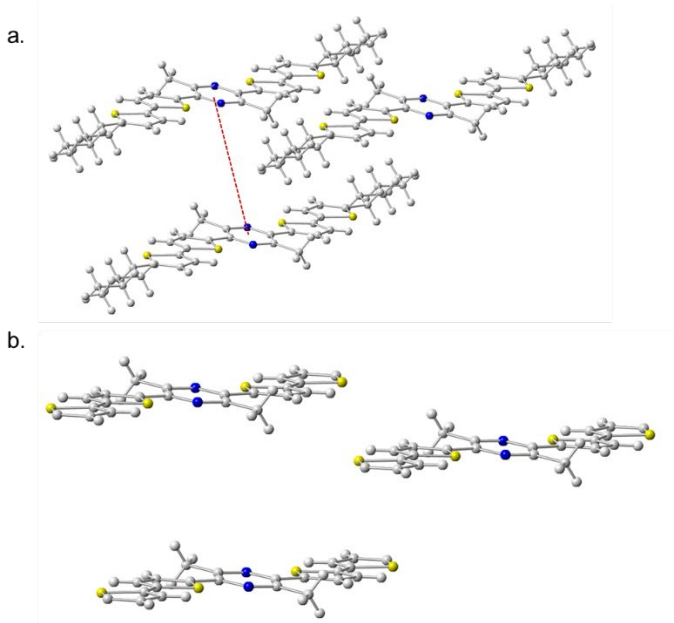

Figure 8. (a) Packing diagram conveying π-stacking of **MePyrz(TT)$_2$**; (b) Crystal fragment detailing the secondary interactions that afford a herringbone arrangement of **MePyrz(TT)$_2$;** red dotted lines correspond to centroid-centroid distance

triclinic $P\overline{1}$ space group where molecules exhibit predominantly co-facial interactions between neighboring molecular frameworks (Fig. 7). The dihedral angle between pyrazine and furan is 176.7° which is less planar compared to **Pyrz(FT)$_2$**. The π-π stacking distance also increased to 3.60 Å (from plane to plane and 5.43 Å, centroid-centroid). This packing arrangement yields a comparatively higher quantum yield (5%) than **Pyrz(FT)$_2$**.

MePyrz(TT)$_2$ also yields crystals in the triclinic $P\overline{1}$ space group; however, with a quantum yield of 12%, we assumed that **MePyrz(TT)$_2$** would have a packing arrangement similar to that of **Pyrz(TT)$_2$** with larger π-π stacking distances between molecules (Fig. 8). Undoubtedly, the stacking distance is larger (4.49Å, from plane to plane; 7.68 Å centroid-centroid); however, no herringbone arrangement was observed. In this case, the molecules display a displaced stacked arrangement, one in which the central π-cores avoid overlapping with each other but rather align with the linear hexyl chain. This packing arrangement is known as lamellar stacking and refers to a separation between the conjugated π-framework and aliphatic chain. The dihedral angle between pyrazine and thiophene is 177.1° where sulfur-nitrogen interaction (S-C-C-N *cisoid* configuration) appears to aid in the planarization of the molecule.

Conclusions

Herein heterocyclic aromatic oligomers based on thiophene, furan, and pyrazine were synthesized and their solid-state arrangements were correlated to spectroscopic properties. Data shows clear trends between electrochemical, theoretical and optical features where even small substitution effects and connectivity selections contribute to optoelectronic behavior. The results of this work highlight the importance of judicious design criteria for materials where favorable optical and photophysical properties can be induced and advanced materials can be achieved.

Acknowledgements

D.K. and D.L.W. appreciate financial support of this work from the National Science Foundation CAREER Award under Grant Number CHE-1652094. N.I.H and A.E.S. appreciate financial support of this work from the National Science Foundation under Grant Number OIA-1539035.

Notes and references

1. A. A. Babaryk, M. Haouas, O. Khaynakova, E. Elkaïm and P. Horcajada, *Crystal Growth & Design*, 2020, **20**, 6510-6518.
2. L. Xing and C. K. Luscombe, *Journal of Materials Chemistry C*, 2021, **9**, 16391-16409.
3. C. Liu, K. Wang, X. Gong and A. J. Heeger, *Chemical Society Reviews*, 2016, **45**, 4825-4846.
4. C. Schmuck and W. Wienand, *Angewandte Chemie International Edition*, 2001, **40**, 4363-4369.
5. R. P. Bisbey and W. R. Dichtel, *ACS Central Science*, 2017, **3**, 533-543.
6. A. Rahmanudin, L. Yao and K. Sivula, *Polymer Journal*, 2018, **50**, 725-736.
7. S. I. Seok, M. Grätzel and N. G. Park, *Small*, 2018, **14**, 1704177.
8. L. Ouahab and E. Yagubskii, *Organic conductors, superconductors and magnets: from synthesis to molecular electronics*, Springer Science & Business Media, 2004.
9. M. Jeffries-EL, B. M. Kobilka and B. J. Hale, *Macromolecules*, 2014, **47**, 7253-7271.
10. G. Turkoglu, M. E. Cinar and T. Ozturk, *Sulfur Chemistry*, 2019, 79-123.
11. N. E. Shevchenko, V. G. Nenajdenko and E. S. Balenkova, *Synthesis*, 2003, **2003**, 1191-1200.
12. E. Marseglia, F. Grepioni, E. Tedesco and D. Braga, *Molecular Crystals and Liquid Crystals Science and Technology. Section A. Molecular Crystals and Liquid Crystals*, 2000, **348**, 137-151.
13. Y. Shlmlzu and T. Azuml, *The Journal of Physical Chemistry*, 1982, **86**, 22-26.
14. A. S. Shetty, J. Zhang and J. S. Moore, *Journal of the American Chemical Society*, 1996, **118**, 1019-1027.
15. O. Gidron and M. Bendikov, *Angewandte Chemie International Edition*, 2014, **53**, 2546-2555.
16. H. Shang, H. Shimotani, S. Ikeda, T. Kanagasekaran, K. Oniwa, T. Jin, N. Asao, Y. Yamamoto, H. Tamura and K. Abe, *The Journal of Physical Chemistry C*, 2017, **121**, 2364-2368.
17. H. Tamura, I. Hamada, H. Shang, K. Oniwa, M. Akhtaruzzaman, T. Jin, N. Asao, Y. Yamamoto, T. Kanagasekaran and H. Shimotani, *The Journal of Physical Chemistry C*, 2013, **117**, 8072-8078.
18. O. Gidron, N. Varsano, L. J. Shimon, G. Leitus and M. Bendikov, *Chemical Communications*, 2013, **49**, 6256-6258.
19. K. Oniwa, T. Kanagasekaran, T. Jin, M. Akhtaruzzaman, Y. Yamamoto, H. Tamura, I. Hamada, H. Shimotani, N. Asao and S. Ikeda, *Journal of Materials Chemistry C*, 2013, **1**, 4163-4170.
20. Y. Li, G. Vamvounis and S. Holdcroft, *Macromolecules*, 2002, **35**, 6900-6906.
21. G. Barbarella, M. Zambianchi, L. Antolini, P. Ostoja, P. Maccagnani, A. Bongini, E. A. Marseglia, E. Tedesco, G. Gigli and R. Cingolani, *Journal of the American Chemical Society*, 1999, **121**, 8920-8926.
22. C. Lee, W. Yang and R. G. Parr, *Physical Review B*, 1988, **37**, 785-789.
23. B. Miehlich, A. Savin, H. Stoll and H. Preuss, *Chemical Physics Letters*, 1989, **157**, 200-206.
24. A. D. Becke, *The Journal of Chemical Physics*, 1993, **98**, 5648-5652.
25. R. Krishnan, J. S. Binkley, R. Seeger and J. A. Pople, *The Journal of Chemical Physics*, 1980, **72**, 650-654.
26. A. D. McLean and G. S. Chandler, *The Journal of Chemical Physics*, 1980, **72**, 5639-5648.
27. M. E. Casida, C. Jamorski, K. C. Casida and D. R. Salahub, *The Journal of Chemical Physics*, 1998, **108**, 4439-4449.
28. R. E. Stratmann, G. E. Scuseria and M. J. Frisch, *The Journal of Chemical Physics*, 1998, **109**, 8218-8224.
29. C. Van Caillie and R. D. Amos, *Chemical Physics Letters*, 1999, **308**, 249-255.

30. R. Bauernschmitt and R. Ahlrichs, *Chemical Physics Letters*, 1996, **256**, 454-464.
31. M. Pourbaix, *NACE*, 1974, **307**.
32. Y. Zhang, S. A. Autry, L. E. McNamara, S. T. Nguyen, N. Le, P. Brogdon, D. L. Watkins, N. I. Hammer and J. H. Delcamp, *The Journal of Organic Chemistry*, 2017, **82**, 5597-5606.
33. G. E. Tyson, K. Tokmic, C. S. Oian, D. Rabinovich, H. U. Valle, T. K. Hollis, J. T. Kelly, K. A. Cuellar, L. E. McNamara and N. I. Hammer, *Dalton Transactions*, 2015, **44**, 14475-14482.
34. G. Sheldrick, *Acta Crystallographica Section A*, 2008, **64**, 112-122.
35. O. V. Dolomanov, L. J. Bourhis, R. J. Gildea, J. A. K. Howard and H. Puschmann, *Journal of Applied Crystallography*, 2009, **42**, 339-341.
36. A. Bolduc, S. Dufresne, G. S. Hanan and W. Skene, *Canadian Journal of Chemistry*, 2010, **88**, 236-246.
37. A. Hucke and M. Cava, *The Journal of Organic Chemistry*, 1998, **63**, 7413-7417.
38. I. P. Koskin, E. A. Mostovich, E. Benassi and M. S. Kazantsev, *The Journal of Physical Chemistry C*, 2017, **121**, 23359-23369.
39. M. A. Perkins, L. M. Cline and G. S. Tschumper, *The Journal of Physical Chemistry A*, 2021, **125**, 6228-6237.
40. A. E. Steen, T. L. Ellington, S. T. Nguyen, S. Balasubramaniam, I. Chandrasiri, J. H. Delcamp, G. S. Tschumper, N. I. Hammer and D. L. Watkins, *The Journal of Physical Chemistry C*, 2019, **123**, 15176-15185.
41. M. Shaker, B. Park, J.-H. Lee, C. K. Trinh, H.-J. Lee, J. woo Choi, H. Kim, K. Lee and J.-S. Lee, *RSC advances*, 2017, **7**, 16302-16310.
42. J.-L. Bredas, *Materials Horizons*, 2014, **1**, 17-19.
43. T.-B. Ren, W. Xu, W. Zhang, X.-X. Zhang, Z.-Y. Wang, Z. Xiang, L. Yuan and X.-B. Zhang, *Journal of the American Chemical Society*, 2018, **140**, 7716-7722.
44. W.-C. Chen, P.-T. Chou and Y.-C. Cheng, *The Journal of Physical Chemistry C*, 2019, **123**, 10225-10236.
45. S. Ahmed and D. J. Kalita, *The Journal of chemical physics*, 2018, **149**, 234906.
46. B. Sk, S. Khodia and A. Patra, *Chemical Communications*, 2018, **54**, 1786-1789.
47. K. Becker, E. Da Como, J. Feldmann, F. Scheliga, E. Thorn Csányi, S. Tretiak and J. Lupton, *The Journal of Physical Chemistry B*, 2008, **112**, 4859-4864.
48. M. D. Curtis, J. Cao and J. W. Kampf, *Journal of the American Chemical Society*, 2004, **126**, 4318-4328.
49. J. Zhang, Q. Zhang, T. T. Vo, D. A. Parrish and J. n. M. Shreeve, *Journal of the American Chemical Society*, 2015, **137**, 1697-1704.
50. D. B. Ninković, G. V. Janjić, D. Veljković, D. N. Sredojević and S. D. Zarić, *Chemphyschem : a European journal of chemical physics and physical chemistry*, 2011, **12**, 3511-3514.
51. P. Kuś, J. Kusz and M. Książek, *Journal of Chemical Crystallography*, 2020, **50**, 21-27.
52. S. T. Kochuveedu and D. H. Kim, *Nanoscale*, 2014, **6**, 4966-4984.
53. Q. Li and Z. Li, *Advanced science*, 2017, **4**, 1600484.